Impact of the Mapping Strategy on the Performance of APP Decoded Space–Time Block Codes

Aydin Sezgin, *Member, IEEE* and Eduard A. Jorswieck, *Member, IEEE*

***Abstract*—In this paper, we propose a "turbo" coding scheme consisting of the serially concatenation of a channel code and OSTBC with iterative processing at the receiver. We analyze the impact of different mapping strategies on the information transfer of the space–time detector with EXIT-charts and derive some criteria for the optimum mapping strategy.**

***Index Terms*—EXIT-charts, iterative decoding, mapping, space–time codes.**

I. Introduction

RECENT information theoretic results have demonstrated that the capacity of the channel in the presence of Rayleigh fading improves significantly by using multiple transmit and receive antennas [1]–[3]. Since then there has been considerable work on a variety of space–time coding schemes. More recently, the authors in [4]–[6] proposed to use a powerful channel code (e.g., turbo codes [7]) in concatenation with a space–time unitary matrix differential modulation code or orthogonal space–time block codes (OSTBC) [8], [9] in order to achieve significant coding gains. STBC from orthogonal design provide the maximum possible diversity gain for a multiple-input–multiple-output (MIMO) channel, but no coding gain.

In this work, we consider the concatenation of an outer code with OSTBC [9] as the inner code in order to improve the performance of the uncoded system, and in order to approach the capacity promised by the information theoretic results. Differently from [4], [5], decoding at the receiver is done in an iterative manner between the soft-input–soft-output (SISO) space–time detector and the SISO channel decoder. We consider different mapping strategies and analytically show that it is possible to improve the performance by employing other mapping schemes than Gray mapping. Furthermore, we derive some mapping criteria to obtain better performance for iterative decoding. Very recently, mapping strategies for turbo detection have also been investigated and optimized with respect to different criteria in [10]. We analyze the space–time detection and decoding components with extrinsic information transfer (EXIT) charts, which have been proposed in [11] as a quasianalytical tool for predicting the convergence behavior and the performance of concatenated coding systems. An EXIT chart consists of a pair of curves which represent the mutual information transfer functions or transfer characteristics of the component detectors and decoders in the turbo process. Each transfer characteristics is essentially a plot of the a priori mutual information I_A against the extrinsic mutual information I_E for the component decoder of interest. The terms I_A and I_E are related to the probability density functions (pdfs) of the log-likelihood ratios λ_A for the a priori information and λ_E for the extrinsic information, the signal-to-noise ratio E_b/N_0 and the structure of the detector or decoder. The required pdfs can be estimated by generating histograms $p(\lambda_A)$ and $p(\lambda_E)$ of λ_A and λ_E, respectively, for a particular value of E_b/N_0.

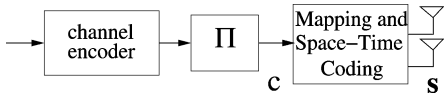

Fig. 1. Model of the transmitter with channel encoder, interleaver, mapper and space–time block coder.

The contribution of this work is the following:

- analysis of the performance of OSTBC within an iterative decoding scheme;
- application of both mutual information and EXIT charts to facilitate the choice of an optimal mapping for OSTBC;
- derivation of two design criteria for optimal mapping.

II. System Model

We consider a system with n_T transmit and n_R receive antennas. We combine a OSTBC with a channel code in serial via a pseudo random interleaver in order to achieve low probability of error for small signal-to-noise-ratios (SNRs). As shown in Fig. 1, after the encoding and interleaving step the F_L coded bits in the bit sequence $\{c_1, \ldots, c_{F_L}\}$, where F_L denotes the frame length, are mapped onto symbols $s \in \mathcal{C}$ from a given constellation $\mathcal{C}$, e.g., M-PSK.

The function $s = f(\mathbf{c})$ describes the mapping of $m = \log_2(M)$ consecutive bits contained in the vector $\mathbf{c}$ onto one constellation symbol s. The symbols s are then space–time coded according to the $p \times n_T$ space–time generator matrix $\mathcal{G}_{n_T}$ or $\mathcal{H}_{n_T}$ [9]. The code rate R is given by $R = q/p$, where q is the number of different symbols and p is the number of time

Manuscript received March 5, 2004; revised February 1, 2005. This work was supported in part by the German Ministry of Education and Research (BMBF) under Grant 01BU150. Part of this work was presented at the IEEE Information Theory Workshop (ITW'03), March 30- April 4, Spring 2003, Paris, France and at the IEEE International Symposium on Information Theory (ISIT'03), Yokohama, Japan, June 29 – July 4, 2003. The associate editor coordinating the review of this manuscript and approving it for publication was Prof. Sheila S. Hemami.

The authors are with the Department of Broadband Mobile Communication Networks, Fraunhofer Institute for Telecommunications, HHI, D-10587 Berlin, Germany (e-mail: aydin.sezgin@hhi.fhg.de; eduard.jorswieck@hhi.fhg.de).

Digital Object Identifier 10.1109/TSP.2005.859243

samples. At the SISO receiver, we apply iterative detection and decoding as described in [12]. Our system model is defined by

$$r_t^j = \sum_{i=1}^{n_T} h_{i,j} s_t^i + n_t^j \tag{1}$$

where r_t^j is the received signal at time t and receive antenna j, s_t^i is the transmitted signal from a given constellation at time t and transmit antenna i, $h_{i,j}$ is the complex channel path gain from transmit antenna i to receive antenna j and n_t^j is a complex Gaussian random variable at time t and receive antenna j. The real and imaginary parts of n_t^j are independent and Gaussian $\mathcal{N}(0, n_T/(2\,\mathrm{SNR}))$ distributed.

The real and imaginary parts of the channel gains are independent and Gaussian distributed random variables with $\mathcal{N}(0, 1/2)$ per dimension. The average energy of the symbols transmitted from each antenna is denoted as E_s, so that the average power of the received signal at each antenna is $n_T E_s$ and the signal-to-noise-ratio is E_s/N_0. Throughout the paper, we assume that the channel path gains are i.i.d. (identically independent distributed) and that successive blocks of channel realizations are independent. The effect of spatial correlation among antennas on the performance of space–time codes is studied in [13], [14]. We further assume that perfect channel state information (CSI) is available at the receiver and that the transmitter has no CSI.

III. Impact of Different Mapping on the Performance

In the following, we analyze the impact of different mappings on the transfer characteristics of the detector for an AWGN channel. The extension to a Rayleigh-fading channel is straightforward. The mutual information between transmitted constellation symbol $s = f(\mathbf{c})$ and received AWGN channel output r is given by (assuming that all constellation symbols are equiprobable)

$$I(S;R) = \frac{1}{M}\sum_{n=1}^{M}\int_{-\infty}^{\infty} p(r|s=s_n) \times \log_2 \frac{p(r|s=s_n)}{p(r)}\, dr \tag{2}$$

with conditional probability density function (pdf)

$$p(r|s=s_n) = \frac{1}{\pi\sigma^2}\exp\left(-\frac{|r-s_n|^2}{\sigma^2}\right) \tag{3}$$

and

$$p(r) = \frac{1}{M}\sum_{n=1}^{M} p(r|s=s_n) \tag{4}$$

where $\log_2(\cdot)$ denotes the base 2 logarithm and σ^2 is the noise variance. With the chain rule of mutual information it can be shown that the mutual information can be decomposed into

$$I(S;R) = I(\mathbf{C};R) = I(C_1,\ldots,C_m;R) = \sum_{L=0}^{m-1} I_L^f \tag{5}$$

where I_L^f is the average mutual information [15], when L bits are already known to the receiver. Note that, the I_L^f depend on the mapping function $f(\cdot)$.

A. Example

For 8PSK ($m = 3$), we have

$$I_0^f = \frac{1}{m\binom{m-1}{0}}\sum_{i=1}^{m} I^f(C_i;R)$$

$$I_1^f = \frac{1}{m\binom{m-1}{1}}\sum_{i=1}^{m}\sum_{\substack{j\neq i\\ j=1,}}^{m} I^f(C_i;R|C_j)$$

$$I_2^f = \frac{1}{m\binom{m-1}{2}}\sum_{i=1}^{m}\sum_{\substack{j=1,\\ j\neq i}}^{m}\sum_{\substack{k\neq i\\ k=j+1,}}^{m} I^f(C_i;R|C_j,C_k)\,.$$

Note that conditioning (i.e., increasing *a priori* knowledge) increases the mutual information, i.e., $I_L^f \geq I_{L-1}^f$. Further note, that the sum in (5) itself is independent of the mapping strategy $s = f(\mathbf{c})$, but that is not the case for the addends. Depending on the constellation $\mathcal{C}$ in use, there are in principal $|\mathcal{C}|!$ different mapping strategies. The question here is how to find a mapping strategy with a good performance in iterative decoding? Before answering the question, let us introduce the subsets $\mathcal{G}_i^+$ and $\mathcal{G}_i^-$, where $\mathcal{G}_i^+ = \{s : c_i = 0\}$ is the set of symbols such that $c_i = 0$ and $\mathcal{G}_i^- = \{s : c_i = 1\}$ is the set of symbols such that $c_i = 1$ for any i with $1 \leq i \leq m$. In order to find some criteria for the optimal mapping strategy with respect to iterative decoding, we are going to analyze the impact of the mapping on I_0^f and I_{m-1}^f from (5), which are the most important addends in the sum.

I_0^f: Let us start with I_0^f, which consists of the weighted sum of mutual information $I^f(C_i;R)$

$$I_0^f(C_i;R) = \frac{1}{2}\left(I^f(C_i;R|c_i=0) + I^f(C_i;R|c_i=1)\right), 1 \leq i \leq m$$

and $I^f(C_i;R|c_i = 0)$ (and similar for $I^f(C_i;R|c_i = 1)$) is given as

$$I^f(C_i;R|c_i=0) = \int_{-\infty}^{\infty} p_i^+(r)\log_2\left(\frac{p_i^+(r)}{p(r)}\right) dr \tag{6}$$

where

$$p_i^+(R) = \frac{2}{M}\sum_{\mathcal{G}_i^+}\frac{1}{\pi\sigma^2}e^{-|R-s|^2/\sigma^2}.$$

The expression in (6) can be only numerically evaluated. However, in order to get more insight, how to choose the mapping strategy, a closed-form expression is needed. With $\log(x) \approx x-1$, x around one, and

$$\frac{p_i^+(R)^2}{p(R)} \approx M\pi\sigma^2 p_i^+(R)^2 \tag{7}$$

after some manipulations, (6) can be approximated by

$$I^f(C_i;R|c_i=0) \approx \frac{1}{2\log(2)}\left(1 + \sum_{s_l\in\mathcal{G}_i^+}\sum_{s_k\in\mathcal{G}_i^+\setminus\{s_l\}} e^{-(1/2)|s_l-s_k|^2/\sigma^2}\right). \tag{8}$$

The approximation in (7) is allowed, since (6) depends strongly on $p_i^+(R)$.

I^f_{m-1}: Similar to I^f_0, I^f_{m-1} consists of a weighted sum of different conditioned mutual information $I^f_{m-1}(C_i; r|\mathbf{C}\backslash\{C_i\})$, which are given as

$$\begin{aligned} &I^f_{m-1}(C_i; R|\mathbf{C}\setminus\{C_i\}) \\ &\quad= \frac{1}{2}(I^f(C_i; R|c_i=0, \mathbf{c}\setminus\{c_i\}) + I^f(C_i; R|c_i=1, \mathbf{c}\setminus\{c_i\})) \\ &\quad= \frac{1}{2}\int_{-\infty}^{\infty} p_{s^+}(r)\log_2\left(\frac{p_{s^+}(r)}{p_{\pm}(r)}\right)dr \\ &\qquad+ \frac{1}{2}\int_{-\infty}^{\infty} p_{s^-}(r)\log_2\left(\frac{p_{s^-}(r)}{p_{\pm}(r)}\right)dr \end{aligned}$$

where $p_{s^+}(R)$ is defined (and similar for $p_{s^-}(R)$) as

$$p_{s^+}(R) = \frac{1}{\pi\sigma^2}e^{-|r-s^+|^2/\sigma^2}$$

where $s^+ = f(c_1, \ldots, c_i = 0, \ldots, c_m)$ (and similar for s^-) and $p_{\pm}(R)$ is defined as

$$p_{\pm}(R) = \frac{1}{2}\left(p_{s^+}(R) + p_{s^-}(R)\right).$$

Again, with $\log(x) \approx x - 1$ and after some manipulations, we arrive at

$$\begin{aligned} &I^f_{m-1}(C_i; R|\mathbf{C}\setminus\{C_i\}) \\ &\qquad\approx -\frac{2\log(\pi\sigma^2)}{\log(2)} - \frac{1}{2}\frac{1+e^{-(1/2)|s^+-s^-|^2/\sigma^2}}{\log(2)\pi\sigma^2}. \end{aligned} \quad (9)$$

From (8) and (9), we can now derive two important mapping strategy criteria. The first criteria is with respect to I^f_{m-1}, say the most right point in the EXIT-charts . In order to achieve low BER with iterative decoding, I^f_{m-1} should be as high as possible. Therefore, in order to achieve a high I^f_{m-1} (see (9)), the first criteria is to get constellation points, which differ in only one symbol bit, as far away as possible from each other.

A highly important fact is that the transfer characteristics of mapping devices are almost straight lines and that the areas under the characteristics are equal [16], [17]. The only difference between different mapping strategies is the slope of the transfer characteristic. Therefore, increasing the right most point of a transfer characteristic results in a decreasing I^f_0, the left most point in the EXIT-chart. The second criteria is with respect to I^f_0. In order to further reduce I^f_0 (see (8)) and automatically enhance I^f_{m-1}, constellation points, which have a symbol bit in common, should be again as far away as possible from each other.

B. Example

In Table I, we show the mapping function $f(\mathbf{c})$ for five different mappings, which we choose from all possible 8PSK mappings [15]. The constellation positions given in Table I are depicted in Fig. 2 for illustration. Note that the mapping strategies "d23" and anti Gray fulfil best the criteria which we mentioned above. Comparing the information transfer for different mappings in Table II, we see that for Gray mapping the difference between I^f_2 and I^f_0 is not as large as in the case of the other mappings. This means that increasing *a priori* knowledge has only small impact on the information transfer of the detector for Gray mapping. Interestingly, this is not true for the other mappings. Here, we observe an improved information transfer by increasing the *a priori* knowledge. Additionally, I^f_0 is larger with Gray mapping in comparison to the other mappings. Therefore, we expect a better performance with Gray mapping in the case, where no *a priori* knowledge is available at the receiver. In addition to the exact values, the approximations of I^f_0 and I^f_2 from (8) and (9) are given in Table II. We observe that the approximations have (qualitative) the same behavior as their exact counterparts, e.g., the approximation of I^f_0 is highest for Gray, reduces gradually and is lowest for anti Gray mapping, which shows that the criteria in (8) and (9) are very useful.

TABLE I
$f(\mathbf{c})$ FOR 5 DIFFERENT MAPPINGS WITH 8PSK

8PSK Mappings					constellation
Gray	natural	"d21"	"d23"	anti Gray	position
000	000	000	000	000	1
001	001	011	011	111	2
011	010	101	101	001	3
010	011	110	110	110	4
110	100	111	001	011	5
111	101	001	010	100	6
101	110	010	100	010	7
100	111	100	111	101	8

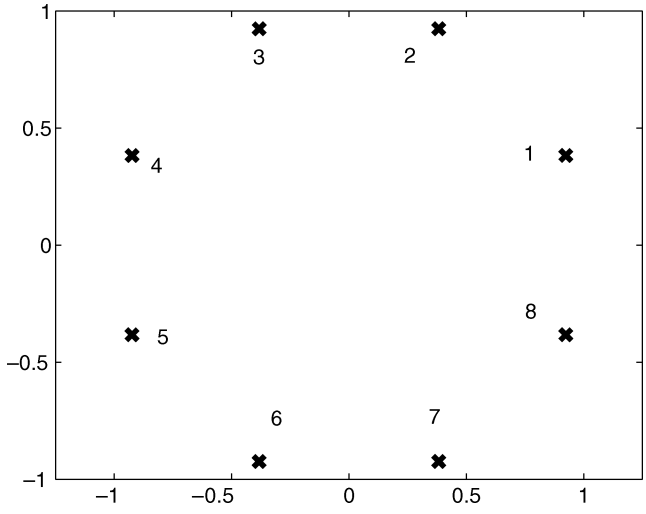

Fig. 2. 8PSK-constellation.

TABLE II
CONDITIONAL MUTUAL INFORMATION I_L FOR DIFFERENT 8PSK MAPPINGS AT $E_b/N_0 = 6$ dB

8PSK mappings	I_L					$\sum I_L = I(s;r)$
	I_0	I_0 (approx.)	I_1	I_2	I_2 (approx.)	
Gray	0.7805	0.3371	0.7819	0.7830	0.1615	2.345
natural	0.6369	0.2128	0.8265	0.8819	0.2087	2.345
"d21"	0.6321	0.2116	0.7736	0.9395	0.2209	2.345
"d23"	0.5380	0.1292	0.8182	0.9889	0.2405	2.345
anti Gray	0.4933	0.0886	0.8723	0.9796	0.2399	2.345

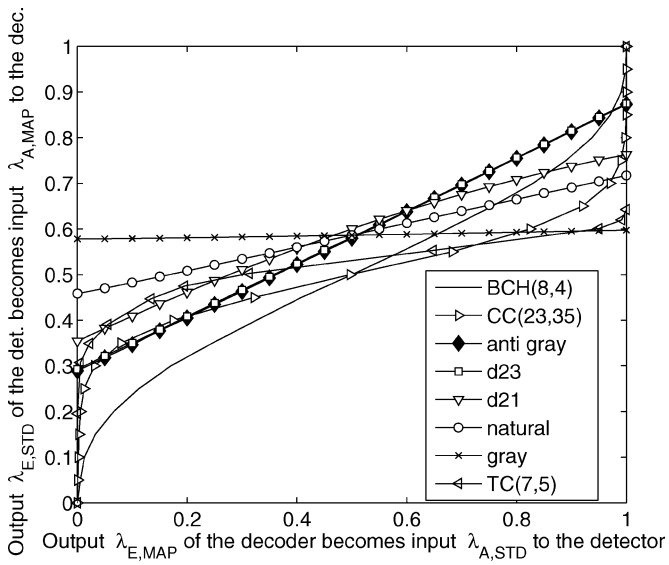

Fig. 3. Extrinsic information transfer (EXIT) charts of outer rate $R_{\text{out}} = 1/2$ decoder and transfer characteristics of inner detector with different mappings.

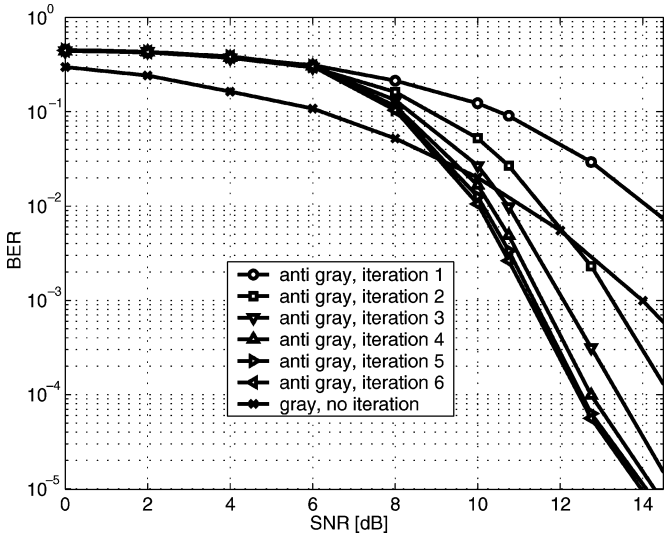

Fig. 4. Performance of the considered outer code [extended BCH(8,4)] in concatenation with the OSTBC $\mathcal{H}_3$ with different mapping strategies, $n_T = 3$ transmit and $n_R = 1$ receive antennas, 8PSK modulation.

IV. EXIT-Chart Analysis

Fig. 3 shows the extrinsic information transfer characteristics of the extended block code BCH(8, 4), the convolutional code CC(23, 35) and the turbo code (TC) (with two recursive CC(7, 5)), all with outer rate $R_{\text{out}} = 1/2$. Additionally, the curves of the space–time detector for $\mathcal{H}_3$ as the inner decoder for different mapping strategies are depicted. The results for other OSTBC such as the Alamouti code [8], $\mathcal{G}_3$, $\mathcal{G}_4$ and $\mathcal{H}_4$ [9] are similar and therefore omitted. Different mappings result in transfer characteristics of different slopes. It is important to know that for the EXIT chart predictions on code performance we assumed very large interleavers and a fast fading channel, in which the channel is selected independently for each space–time code matrix (i.e., channel is constant for only p channel uses). However, in practice using large interleavers is not applicable. In our bit error rate simulations later on in this section we use moderate interleaver sizes. Due to this both assumptions the EXIT charts can be regarded only as asymptotic results. Therefore, the "turbo-cliff"-region occurs not exactly at the predicted SNR values. Note that the detector transfer characteristics are almost straight lines and that at low SNR values increasing the SNR just shifts the curve up. Additionally, note that for high SNR values, the slope of the detector transfer characteristics is also affected (not depicted here). From the figure, we see also that the natural mapping provides good extrinsic output at the beginning but provides diminishing output for higher *a priori* input λ_A. For the antigray mapping it is the other way around. The detector which uses gray mapping provides almost the same extrinsic output for all *a priori* input, which confirms the results from Table II in Section III. Therefore, we expect that the performance of the detector with gray and natural mapping is good in the low SNR regime and for a few iterations in comparison to the other mappings. But in the high SNR regime and for more iterations, we expect that it is the other way around. Note that the axes are swapped for the outer code: λ_A is on the ordinate, λ_E on the abscissa. By comparing the transfer characteristics of the outer codes, we observe that the BCH first surmount the intersection with the detector curves, followed by the CC and then the TC. Thus, we expect that the turbo cliff positions in the BER charts are also in the same order.

Remark 4.1: Notice that the EXIT-chart analysis assumes that the log-likelihood ratios of the bits are Gaussian distributed. Although, that does not exactly hold for the detector considered here, it was shown in [18] that the shape of the involved distributions is only of minor importance for the EXIT-chart analysis. This justifies the application of EXIT-charts for our case.

V. Simulation Results

In this section, the simulation results of the proposed schemes and their interpretation are presented.

For verification of the observations from the EXIT-Charts, we present the bit error rates (BERs) for gray and anti gray mapping in Fig. 4 for a system employing the OSTBC $\mathcal{H}_3$ with $n_T = 3$ transmit and $n_R = 1$ receive antenna. Since the transfer characteristics of all other mapping strategies are almost always between the transfer characteristics of gray and anti gray mapping, only their BERs are depicted. Coding is performed over multiple block fading channels. The transmitted bits are organized in frames of length $F_L = 432$. We assume that one block fading channel is constant for $\tau = 24$ channel uses. We observe that although the curves are relatively flat at iteration 1, there is a significant improvement with further iterations. However, in the case of gray mapping iteratively decoding yields negligible gain, so only the first iteration is plotted. Furthermore, simulation results show, that there occurs a saturation of the improvement for the other mappings beyond iteration 6. This behavior can be explained by the fact that after each iteration the extrinsic output of the receiver components tends to a Gaussian distribution according to the central limit theorem (CLT), but the correlation between the extrinsic information and the channel output increases after each iteration [19]. Hence, the improvement of the BER-performance diminishes after each iteration. In the low SNR regime, however, intersection of the EXIT-curves

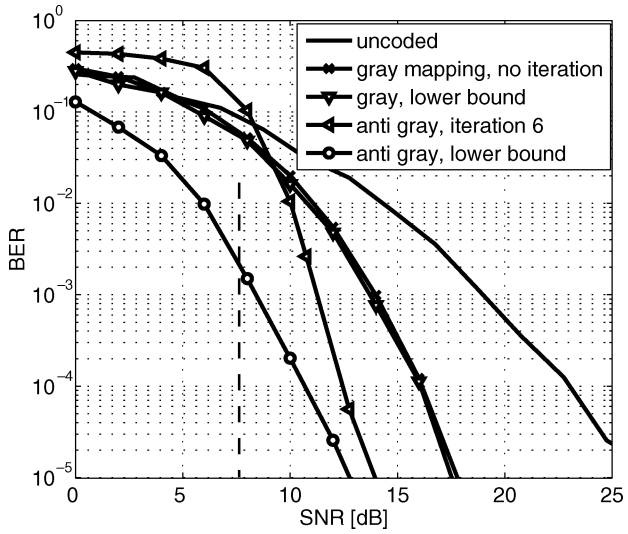

Fig. 5. Performance comparison of the coded and uncoded system, OSTBC $\mathcal{H}_3$ $n_T = 3$ transmit and $n_R = 1$ receive antennas, 8PSK modulation. The dashed line indicates the capacity limit.

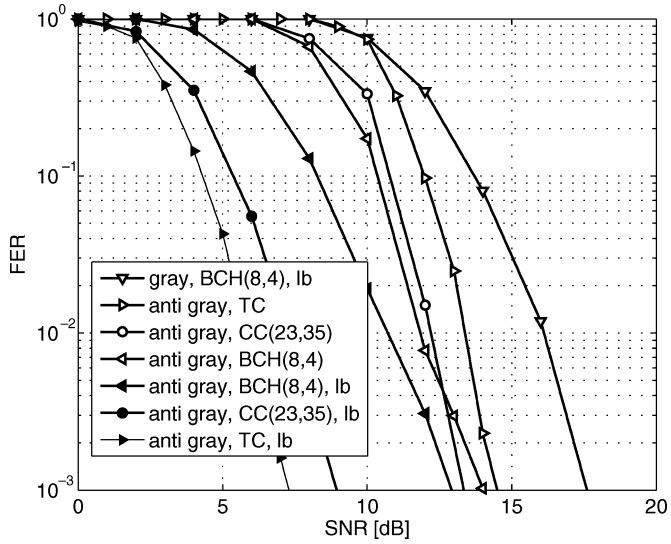

Fig. 6. Frame error rate of the proposed scheme with different outer codes and mapping strategies, lower bound (lb) stands for assumption of perfect *a priori* information.

is the main cause for the poor performance. As predicted in the EXIT-Charts, the BER-performance of the gray mapping is better than the BER-performance of the anti gray mapping in the low SNR regime. In the high SNR regime, however, it is the other way around. Note that this performance difference to gray mapping can further enhanced with a larger frame length or a smaller τ.

To avoid an overload of Fig. 4, the BERs for the uncoded system with gray mapping and coded system with anti gray and gray mapping are depicted in Fig. 5 for comparison. Furthermore, the cases, where we have assumed, that the STD has perfect a priori information are also depicted, to serve as lower bounds. From this figure, we see that there is a significant performance gain compared to the uncoded system. In addition to this, we observe that the performance of the scheme depends strongly on the accuracy of the a priori information in the case of anti Gray mapping, but not for Gray mapping. This also verify our analysis from the EXIT-charts. The performance of the anti Gray scheme with the assumption of perfect a priori information is about 4 dB better at a BER of 10^{-2} than without this assumption. Note that this difference gets smaller for high SNR, since the accuracy of the a priori information in the nonperfect case gets even better for increasing SNR. The dashed line in Fig. 5 indicates the capacity limit. We observe that, at the BER of 10^{-4}, the proposed scheme performs within 6 dB of the capacity. Note that the degradation with respect to capacity is mainly caused by the inner OSTBC.

By using a more powerful channel code such as the 16-state trellis code CC(23, 35) or the turbo code TC(7, 5), the performance with perfect a priori information is even better as depicted in Fig. 6. However, since the transfer characteristics of the CC(23, 35) and the TC(7, 5) do not match as well as the BCH code to the transfer characteristics of the detector, the performance without perfect a priori information is worse in comparison to the BCH code for small SNR, due to the inferior exchange of a priori information between detector and decoder. Further, the turbo cliff position is first achieved by the BCH, followed by the CC and the TC as predicted by the EXIT-chart analysis. On the other hand, for high SNR values, the information transfer between the more powerful codes (CC and TC) and the detector is better and convergence to the right upper corner of the EXIT-chart (area with low BER [11]) is faster obtained. Thus, for higher SNR and better feedback information, the performance of the CC(23, 35) gets better than that of the BCH code. We also observe, that in case of the FER, differently to the BER, the performance with anti-Gray mapping is always better than the Gray mapping strategy for the whole range of SNR values.

VI. Conclusion

In this paper, the serial concatenation of an outer code with different orthogonal space–time block codes has been proposed. We analyzed the impact of different mapping strategies on the information transfer of the SISO detector and analytically showed that additional performance gain is achieved in comparison to Gray mapping. Furthermore, we derived two simple design criteria for the optimal mapping strategy. The performance of this scheme was investigated with EXIT-charts and error rates and compared with the uncoded scheme in [20]. Simulation results show that this scheme performs significantly better in terms of bit error rates in comparison to the uncoded system.

References

[1] E. Telatar, "Capacity of multi-antenna Gaussian channels," *European Trans. Telecommun. ETT*, vol. 10, no. 6, pp. 585–596, Nov. 1999.

[2] G. J. Foschini and M. J. Gans, "On limits of wireless communications in a fading environment when using multiple antennas," *Wireless Pers. Commun.*, vol. 6, no. 3, pp. 311–335, Mar. 1998.

[3] E. Biglieri, G. Caire, and G. Taricco, "Limiting performance of block-fading channels with multiple antennas," *IEEE Trans. Inf. Theory*, vol. 47, no. 4, pp. 1273–1289, May 2001.

[4] G. Bauch, "Concatenation of space-time block codes and TURBO-TCM," in *IEEE Int. Conf. on Communications*, vol. 2, Vancouver, BC, Canada, Jun. 6–10, 1999, pp. 1202–1206.

[5] T. H. Liew and L. Hanzo, "Space-time codes and concatenated channel codes for wireless communications," *Proc. IEEE*, vol. 90, pp. 187–219, Feb. 2002.
[6] A. Steiner, M. Peleg, and S. Shamai (Shitz), "Iterative decoding of space-time differentially coded unitary matrix modulation," *IEEE Trans. Signal Process.*, vol. 50, no. 10, pp. 2385–2395, Oct. 2002.
[7] C. Berrou and A. Glavieux, "Near optimum error correcting coding and decoding:Turbo codes," *IEEE Trans. Commun.*, vol. 44, no. 10, pp. 1261–1271, Oct. 1996.
[8] S. M. Alamouti, "A simple transmitter diversity scheme for wireless communications," *IEEE J. Sel. Areas Commun.*, vol. SAC-16, pp. 1451–1458, Oct. 1998.
[9] V. Tarokh, H. Jafarkhani, and A. R. Calderbank, "Space-time block codes from orthogonal designs," *IEEE Trans. Inf. Theory*, vol. 45, no. 5, pp. 1456–1467, Jul. 1999.
[10] G. Bauch and F. Schreckenbach, "How to obtain turbo gains in coherent and noncoherent orthogonal transmit diversity," in *Proc. IEEE PIMRC*, Beijing, China, Sep. 2003, pp. 1988–1992.
[11] S. ten Brink, "Convergence of iterative decoding," *IEE Electron. Lett.*, vol. 35, no. 10, pp. 806–808, May 1999.
[12] A. Sezgin, D. Wübben, and V. Kühn, "Analysis of mapping strategies for turbo-coded space-time block codes," in *Proc. ITW 2003*, Paris, France, Mar. 30–Apr. 4 2003, pp. 103–106.
[13] M. Uysal and C. N. Georghiades, "Effect on spatial correlation on performance of space-time codes," *Inst. Elec. Eng. Lett.*, vol. 37, no. 3, pp. 181–183, Feb. 2001.
[14] E. A. Jorswieck and A. Sezgin, "Impact of spatial correlation on the performance of orthogonal space-time block codes," *IEEE Commun. Lett.*, vol. 8, no. 1, pp. 21–23, Jan. 2004.
[15] S. ten Brink, "Designing iterative decoding schemes with the extrinsic information transfer chart," *AEUE Int. J. Elec. Commun.*, vol. 54, pp. 187–219, Nov. 2000.
[16] A. Ashikhmin, G. Kramer, and S. ten Brink, "Code rate and the area under extrinsic information transfer curves," in *Proc. IEEE Int. Symp. Inform. Theory (ISIT) 2002*, Jun. 30–Jul. 5 2002, p. 115.
[17] ——, "Extrinsic information transfer functions: Model and erasure channel properties," *IEEE Trans. Inf. Theory*, vol. 50, no. 11, pp. 2657–2673, Nov. 2004.
[18] S. ten Brink, "Code characteristic matching for iterative decoding of serially concatenated codes," *Ann. des Télécommun.*, vol. 56, no. 7–8, pp. 394–408, 2001.
[19] J. Hagenauer, E. Offer, and L. Papke, "Iterative decoding of binary and convolutional codes," *IEEE Trans. Inf. Theory*, vol. 42, pp. 429–445, Mar. 1996.
[20] V. Tarokh, H. Jafarkhani, and A. R. Calderbank, "Space-time block coding for wireless communications: Performance results," *IEEE J. Sel. Areas Commun.*, vol. 17, no. 3, pp. 451–460, Mar. 1999.

Aydin Sezgin (S'01–M'05) received the Dipl.-Ing. (M.S.) degree in communications engineering (with distinction) from the University of Applied Sciences, Berlin, Germany, in 2000, and the Dr.-Ing. (Ph.D.) degree (with distinction) in electrical engineering from the Technical University of Berlin (TUB), Germany.

Since 2001, he has been with the Department of Broadband Mobile Communication Networks, Fraunhofer Institute for Telecommunications, Heinrich-Hertz-Institut (HHI). His current research interests are in the area of signal processing and multiple antenna systems, e.g., MIMO transceiver design and space–time coding.

Eduard A. Jorswieck (SM'01–M'04) received the Diplom-Ingenieur (M.S.) degree and Doktor-Ingenieur (Ph.D.) degree, both in electrical engineering and computer science from the Technische Universität Berlin, Germany, in 2000 and 2004, respectively.

Since 2001, he has been with the Fraunhofer Institute for Telecommunications, Heinrich-Hertz-Institut (HHI) Berlin, in the Broadband Mobile Communication Networks Department. His research activities comprises performance and capacity analysis of wireless systems and optimal transmission strategies for single- and multi-user multiple antenna systems.